# In-plane friction behaviour of a ferrofluid bearing

Lampaert, S. G.E.; Fellinger, B. J.; Spronck, J. W.; van Ostayen, R. A.J.

**DOI**
10.1016/j.precisioneng.2018.05.013

**Publication date**
2018

**Document Version**
Final published version

**Published in**
Precision Engineering

Precision Engineering 54 (2018) 163–170

Contents lists available at ScienceDirect

Precision Engineering

journal homepage: www.elsevier.com/locate/precision

# In-plane friction behaviour of a ferrofluid bearing☆

S.G.E. Lampaert*, B.J. Fellinger, J.W. Spronck, R.A.J. van Ostayen

ARTICLE INFO

*Keywords:*
Precision engineering
Fluid dynamics
Magnetics
Viscous damping
Modelling

ABSTRACT

Ferrofluid bearings have been demonstrated to be very interesting for precision positioning systems. The friction of these bearings is free of stick-slip which results in an increase of precision. More knowledge on the friction behaviour of these bearings is important for there application in precision positioning systems. This paper demonstrates that the friction of a ferrofluid bearing can be modelled by a viscous damper model and provides a basic model to predict the friction behaviour of a bearing design. The model consists of a summation of a Couette flow with a Poiseuille flow such that there is no net fluid transport under the bearing pads. The model is experimentally validated on a six degrees of freedom stage using ferrofluid bearings. A stiffness in the form of a closed-loop control gain is introduced in the system to create a resonance peak at the desired frequency. The damping coefficient can be identified from the peak height of the resonance, since the peak height is the ratio of total energy to dissipated energy in the system. The results show that the newly derived model can be used to make an estimate of the damping coefficient for small(~ 1 mm) stroke translations. Furthermore, the model shows that the load capacity of a ferrofluid pocket bearing is affected during sliding.

## 1. Introduction

The repeatability of precision positioning systems can be improved by reducing the effects of stick-slip in system [1]. Stick-slip is the result of a spontaneous jerking motion which is introduced when overcoming the static friction coefficient between two sliding contacts. Bearing concepts like magnetic bearings, fluids bearings and flexures don't have this stick-slip effect but have other drawbacks like complexity, cost, or the storage of energy while moving.

Ferrofluid bearings, first proposed by Rosensweig et al. [2], provide a cost-effective alternative to these more conventional bearing systems. The bearing consist of a magnet and a ferrofluid that are attracted to each other forming a thin layer of ferrofluid inbetween the permanent magnet and the opposing bearing surface (Fig. 1).

The permanent magnet makes it a natural candidate for combination with Lorentz actuators, as demonstrated in various systems [3–15]. The result is a bearing that has distinct advantages for precision positioning systems, such as inherent stability, viscous friction, linear actuation, absence of external equipment, and no discernible stick slip effects. Furthermore, the carrier fluid can be chosen to suit the operating environment and the design allows for a compact, lightweight and cost effective solution.

Ferrofluid bearings have been successfully incorporated in precision positioning systems. Cafe [9,10] has built a six degrees of freedom(DoF) stage with nanometer accuracy, demonstrating that the bearing can be used in high precision positioning systems. Mok [13], Habib [11] and van Moorsel [15] have successfully implemented ferrofluid bearings in combination with low-cost sensor solutions, to capitalize on the cost-effectiveness.

Ferrofluid bearings can be divided into pressure bearings and pocket bearings. The load capacity of a ferrofluid pressure bearing is solely developed by the pressure in the fluid developed by the magnetic bodyforce [16]. The load capacity and stiffness behaviour of ferrofluid pocket bearings have recently been described in Refs. [17–19]. Though, this previous work does not yet include the effect of translating the bearing, nor does it describe the friction of the bearing. Due to this uncertainty that is introduced in the model, Café [9] and Habib [11] have put a large safety factor on the friction forces during the design of the system, resulting in a situation where the friction forces are dominating the disturbance forces.

This paper describes and experimentally validates a basic model of the in-plane friction behaviour of a ferrofluid bearing. It will do so by deriving a model describing the viscous damping forces of a ferrofluid bearing. The model will be experimentally validated on a demonstrator stage.

## 2. Theoretical bearing model

The forces that act on a ferrofluid bearing are found by deriving the flow field between two surfaces from the general Navier-Stokes

☆ This paper was recommended by Associate Editor Gorka Aguirre.

* Corresponding author.
*E-mail address:* s.g.e.lampaert@tudelft.nl (S.G.E. Lampaert).

https://doi.org/10.1016/j.precisioneng.2018.05.013
Received 31 October 2017; Received in revised form 27 March 2018; Accepted 30 May 2018
Available online 09 July 2018

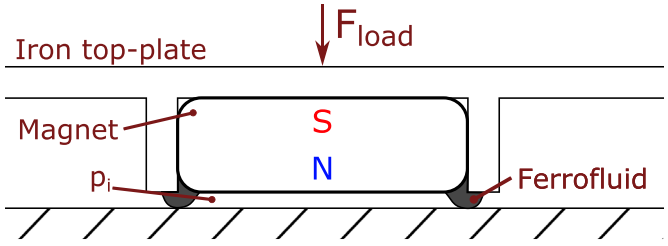


(a) The cross-section of a ferrofluid bearing.

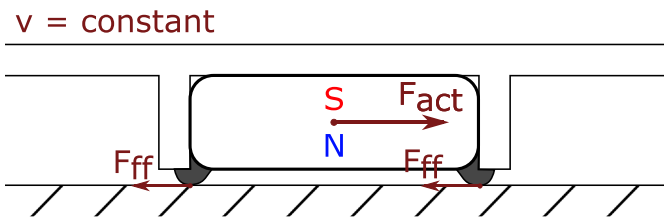


(b) Actuator forces and friction forces.

**Fig. 1.** a shows how a load bearing ring is created by the permanent magnet and ferrofluid, while the iron top-plate increases the magnetic field intensity a the underside. b shows the actuation force and counteracting friction forces for a constant speed.

equation. The flow field is then used to determine the shear stresses in the system which can be related to the friction forces. An analysis of the viscosity of ferrofluids is added to verify the used viscosity model.

### 2.1. Viscosity

The viscosity of a ferrofluid changes when subjected to a magnetic field [20]. This happens due to two different effects: rotational viscosity and particle chain formation. The following section discusses the impact of these effects on the rheology of the fluid.

#### 2.1.1. Rotational viscosity

The effect of rotational viscosity is caused by the alignment of the particles to the magnetic field. This results in a larger effective viscosity when the vorticity is perpendicular to the magnetic field. The viscosity of the fluid using spherical particles can be modelled with the following relation that uses $\eta_c$ for carrier viscosity, $\phi$ for volumetric concentration, $\beta$ for the angle between magnetic field and vorticity, $\mu_0$ for magnetic permeability of vacuum, $m$ for magnetic moment of a ferrofluid particle, $H$ for magnetic field intensity, $k$ for Boltzmann constant and $T$ for temperature [21].

$$\eta = \eta_c\left(1 + \frac{5}{2}\phi + \frac{3}{2}\phi\frac{\alpha - \tanh\alpha}{\alpha + \tanh\alpha}\sin^2\beta\right)$$
$$\alpha = \frac{\mu_0 mH}{kT} \tag{1}$$

The first term of this equation presents the viscosity of the carrier fluid, the second term presents the increase in viscosity due to the suspension of particles and the third term presents the change in viscosity due to the magnetic field. For large values of $\alpha$ this relation has a maximum value of:

$$\eta_{max} = \eta_c\left(1 + \frac{5}{2}\phi + \frac{3}{2}\phi\right) = \eta_c(1 + 4\phi) \tag{2}$$

The viscosity of a ferrofluid is often given in the absence of a magnetic field, the relation for the viscosity then reduces to the Einstein formula [22]:

$$\eta_0 = \eta_c\left(1 + \frac{5}{2}\phi\right) \tag{3}$$

A typical value for the increase in viscosity caused by the effect of rotational viscosity can be calculated by combining relation (2) and (3) and assuming a typical concentration of about $\phi = 8\%vol$.

$$\frac{\eta_{max}}{\eta_0} = \frac{1 + 4\phi}{1 + \frac{5}{2}\phi} = \frac{1 + 4 \times 0.08}{1 + \frac{5}{2}0.08} = 1.1 \tag{4}$$

This relation shows that the increase in viscosity due to the magnetic attraction is in the order of 10%.

#### 2.1.2. Particle chain formation

The particle chain formation, often referred to as the magneto-viscous effect [23], is the formation of chain like structures in the fluid due to the magnetic interaction between the particles. These structures are more difficult to rotate in the fluid resulting in a larger resistance to shear which results in an increase in effective viscosity [24]. Applying a magnetic field on the fluid increases the resistance to rotation even more resulting in an even further increase in viscosity. Shear forces in fluid might break the chains in the fluid resulting in a shear thinning effect. The formation of chains can be investigated by analysing the dipolar interaction parameter λ which is given with the following relation that uses $M_0$ for particle magnetization strength and $V$ for particle volume.

$$\lambda = \frac{\mu_0 m^2}{4\pi kTd^3} = \frac{\mu_0 M_0^2 V}{24kT} \propto d^3 \tag{5}$$

Chain like structures will develop in the fluid when this parameter becomes larger than one. Increasing this parameter results in longer chains in the fluid [25]. The formula shows that λ increases with the diameter $d$ of the particles resulting in only the larger particles contributing to the formation of chains. It has been shown that even a small concentration of large particles in the fluid can cause a high increase of viscosity [26]. For the models presented in this paper, it is key to choose a ferrofluid at which the dipolar interaction parameter is lower than one for all suspended magnetic particles.

### 2.2. Flow field

The geometry of the ferrofluid seal consists of a thin layer of fluid which is held fixed on the magnet against a moving counter surface (see Figs. 1 and 2). The derivation of the flow field starts with the general Navier-Stokes equations for incompressible Newtonian fluids, with an additional term ($\mu_0 M_s \nabla H$) describing the magnetic body forces. The assumption of an Newtonian fluid is reasonable for magnetic fluids with a small effect of rotational viscosity and a small dipolar interaction parameter λ. The relation uses $\vec{u}$ for fluid velocity, $p$ for pressure, $\eta$ for viscosity and $\vec{f}$ for body forces.

$$\rho\left(\frac{\delta\vec{u}}{\delta t} + \vec{u}\cdot\nabla\vec{u}\right) = -\nabla p + \eta\nabla^2\vec{u} + \mu_0 M_s \nabla H + \vec{f}$$
$$\nabla\cdot\vec{u} = 0 \tag{6}$$

For a typical bearing application, the Reynolds number in the flow can be shown to be small as is done in the following relation that uses $L$ for the length of the bearing, $U$ for its speed and ρ is the density of the ferrofluid.

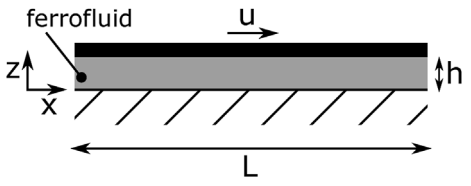


**Fig. 2.** Two large plates($L \gg h$) moving with respect to each other with velocity $u$ and separated with a ferrofluid film with height $h$.

$$\frac{\partial p}{\partial x} = \eta\frac{\partial^2 u_x}{\partial z^2} + \mu_0 M_s \frac{\partial H}{\partial x} \tag{9}$$

$$Re = \frac{\rho UL}{\eta} = \frac{1380 \times 10^{-3} \times 10^{-2}}{0.15} = 0.09 \ll 1 \tag{7}$$

This demonstrates that it is reasonable to neglect the inertial terms. This leads to the Stokes equation given in equation (8) where the magnetic body force is the only body force.

$$\nabla p = \eta \nabla^2 \vec{u} + \mu_0 M_s \nabla H$$
$$\nabla \cdot \vec{u} = 0 \tag{8}$$

The flow field between the bearing pads is modelled as a fluid between two large parallel plates ($L \gg h$) that slide relative to each other, as shown in Fig. 2. Equation (8) can be further reduced to equation (9) by noting that the flow is parallel to the x-axis and by assuming that both the pressure and magnetic field are constant across the film height.

Equation (9) shows that the pressure is the result of the viscous forces and magnetic body forces.

$$\frac{\partial^2 u_x}{\partial z^2} = \frac{1}{\eta}\frac{\partial}{\partial x}(p - \mu_0 MH) \tag{10}$$

For the sake of simplicity, the magnetic body force and the pressure are replaced by the following substitution.

$$\frac{\partial^2 u_x}{\partial z^2} = \frac{1}{\eta}\frac{\partial p^*}{\partial x} \tag{11}$$

Integrating relation (11) twice over the height and introducing the no slip boundary conditions at $z = 0, u = 0$, and $z = h, u = U$ results in the following relation for the velocity profile:

$$u_x = \frac{1}{2\eta}\frac{\partial p^*}{\partial x}(z^2 - hz) + \frac{U}{h}z \tag{12}$$

Translating the bearing causes no net fluid transport under the bearing pads due to the magnetic body force that keeps the ferrofluid in place. This can be used to calculate a value for $\frac{\delta p^\star}{\delta x}$ by setting the integral of the fluid velocity over the fly height $h$ to zero.

$$\int_0^h u_x dz = -\frac{1}{12\eta}\frac{\partial p^*}{\partial x}h^3 + \frac{U}{h}z = 0 \tag{13}$$

and thus:

$$\frac{\partial p^*}{\partial x} = 6\frac{\eta U}{h^2} \tag{14}$$

Which, after substituting in (12), results in the flow field:

$$u_x = 3U\frac{z}{h}\left(\frac{z}{h} - \frac{2}{3}\right) \tag{15}$$

The resulting flow field presented in equation (15) is plotted in Fig. 3. The flow field shows a summation of a Couette flow with a Poiseuille in such a way that there is no net fluid transport. The Couette flow is caused by the translational motion and the Poiseuille flow is the result of the magnetic body force.

### 2.3. Friction force

The friction force can be calculated by integrating the shear stress of the fluid on the bearing surface. The shear stress in the fluid is defined by the velocity gradient between the bearing surfaces and can be determined using the flow field given by relation (15).

$$\tau_{zx} = \eta\frac{\partial u_x}{\partial z} \tag{16}$$

$$= \eta\frac{\partial}{\partial z}\left[3\frac{U}{h}\frac{z^2}{h} - \frac{2z}{3}\right] \tag{17}$$

$$= 6\eta\frac{U}{h}\left(\frac{z}{h} - \frac{1}{3}\right) \tag{18}$$

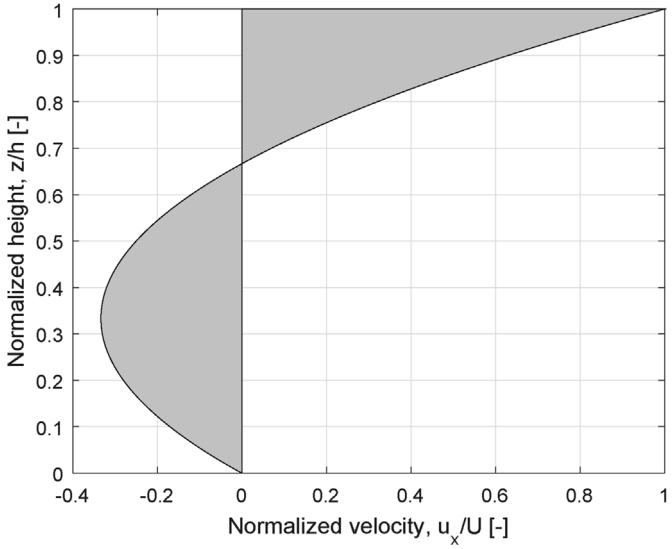


**Fig. 3.** This figure presents the modelled flow field of a ferrofluid bearing during a translational motion, as described in (15). A Couette flow is combined with a counteracting Pouiseuille flow. The flow-field is normalized with respect to the velocity at $z = h$.

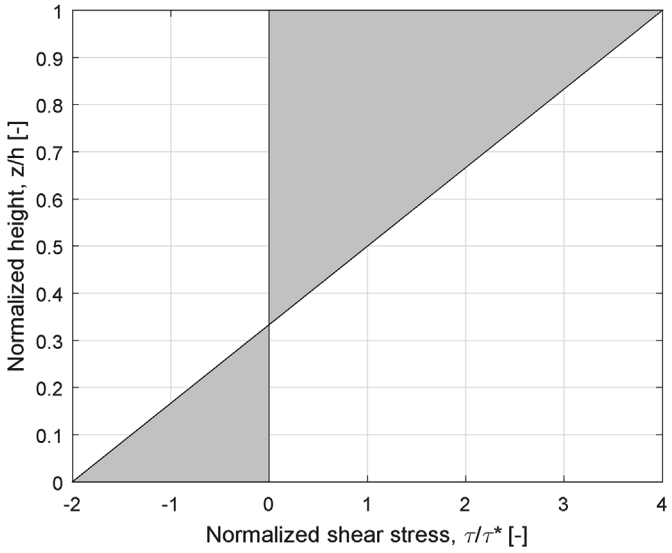


**Fig. 4.** This figure presents the normalized shear stress profile in-between the two bearing surfaces of a ferrofluid bearing, as described in (18). The shear stress is normalized for $\tau^* = \frac{\tau h}{\eta U}$.

A graphical representation of the shear force in-between the two bearing pads is given by Fig. 4. The shear force at the surface of the moving bearing is defining the force on the moving surface. The value of this shear force can be calculated for a value of $z = h$.

$$\tau_{zx} = 4\eta\frac{U}{h} \tag{19}$$

The magnetic body force retaining the ferrofluid at the magnet is found in the factor four, describing the additional forces introduced. The friction at the moving surface can be calculated by integrating the shear stress over the area of the bearing surface.

$$F_{fric} = \int_S \tau_{zx} dA \tag{20}$$

$$= 4\eta\frac{UA}{h} \tag{21}$$

From equation (21) it is apparent that a ferrofluid bearing behaves like a linear viscous bearing. So the damping coefficient can be determined by dividing the friction force by the velocity.

$$c = \frac{F_{fric}}{U} = 4\eta\frac{A}{h} \tag{22}$$

### 2.4. Sealing capacity during translation

According to equation (11) the pressure distribution across a seal is influenced by the viscous effect during translation. A model of this effect can be developed by combining this relation with relation (14).

$$\frac{\partial}{\partial x}(p - \mu_0 MH) = 6\frac{\eta U}{h^2} \tag{23}$$

Based on the work presented in Ref. [17], the pressure difference across a seal can now be calculated the following relation where $l_{seal}$ is the width of the seal in the sliding direction.

$$\Delta p = \mu_0 M\Delta H - \int_0^{l_{seal}} 6\frac{\eta U}{h^2}dx \tag{24}$$

$$= \mu_0 M\Delta H - 6\frac{\eta U}{h^2}l_{seal} \tag{25}$$

In the case of a pocket bearing as introduced in Ref. [17], the maximum load capacity can be modelled with equation (26) where $A_p$ stands for the surface area of the enclosed and pressurised pocket of air carrying the load. The relation shows that shows that the load capacity reduces during a translational motion.

$$F_L = \mu_0 M\Delta H A_p - 6\frac{\eta U}{h^2}l_{seal}A_p \tag{26}$$

This relation for the load capacity of a ferrofluid pocket bearing is an extension of the relation presented in Ref. [17] for situations where the bearing is sliding with a velocity U.

## 3. Experimental method

The damping is both predicted based on the theory presented in the previous chapter and measured using an experimental set-up. Validation of the predicted damping coefficient with the experimental set-up is used to demonstrate that the proposed model is reasonable to predict the friction of a ferrofluid bearing or seal.

### 3.1. Damping coefficient prediction

Based on the theory presented in the previous chapter, the damping coefficient can be predicted by measuring the viscosity, contact surface area and fly height of the bearing. The fly height is measured by taking a foto of the air-gap with a scale next to it. The known scale length is used as a reference in the photograph and related to the length of a single pixel. Then by using a pixel counter the air-gap is measured at several points. The contact area is measured by resting the moving mass against two endstops on a white acrylic sheet. The mass is removed and the imprint left by the bearings is photographed next to a known scale. The length of a pixel is derived from the scale and the resulting surface area is measured using the software ImageJ.

### 3.2. Experimental set-up

The experimental validation will be performed on an improved version of the (2 + 4) degrees of freedom stage of Cafe et al. [9,10]. This is a system that can do large translational motions in x- and y-direction while having the other four degrees of freedom constrained through closed-loop control (Fig. 5). The system is chosen because the different parameters defining the dynamic behaviour (mass, damping and stiffness) are properly defined. The mass is solely defined by the moving mass of the system, the damping is solely defined by the friction of the ferrofluid bearings and the stiffness is solely defined by the applied control stiffness.

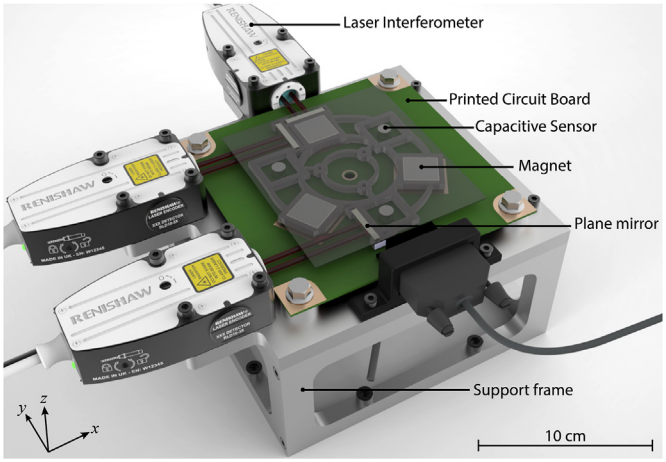


**Fig. 5.** An overview of the general layout of the demonstrator stage on which the experimental validation will be performed. In this figure the moving mass is opaque to better showcase the internal components. The magnets are mounted on the moving mass and are used as a ferrofluid bearing and magnetic field source for actuation. The PCB contains the force generating coils. The in-plane measurements are done with three laser interferometers and the out-of-plane measurements are done with three capacitive sensors underneath the moving mass. The plane mirrors are used as a reference for the laser interferometer and mounted on the moving mass. The support frame is mounted on a vibration isolation table.

The moving mass is used as a reference for the sensors and contains three square magnets, as shown in Fig. 5. The magnets provide the magnetic field both for the ferrofluid bearing and Lorentz actuation. The stage has an in-plane movement range of 10mmx10 mm and the rotation is constrained through control action.

The system has six sensors to sense the principal degrees of freedom of a rigid body. The in-plane motions and rotation are measured by interferometers and the out-of-plane motion and tilts are measured by capacitive sensors. The in-plane position is limited by the sensor resolution of 10 nm. The position is controlled with a bandwidth of 200Hz, while the rotation is controlled with 100Hz. The out-of-plane motions and tilts are measured by three capacitive sensors limited by the noise level of 2.54 nm at a sampling frequency of 10 kHz. They are constrained through closed-loop control using three out-of-plane Lorentz actuators and with a bandwidth of 200 Hz.

The actuation is performed by two sets of three Lorentz actuators embedded in a multi-layered PCB. Fig. 6 shows how the coils are configured to create resultant in-plane and out-of-plane forces for a non-uniform magnetic field. The in-plane control actuation has a motor constant of 0.145 $NA^{-1}$. The motor-constant of the experimental set-up is determined with a load-cell test in the direction of the movement. The test is conducted by applying a current to the in-plane coils, such that the moving mass enacts a force in line with the load cell. The current is increased to map the data points, which are then fitted to find the motor constant.

The closed-loop system is identified by supplying a pseudo random white noise signal with an amplitude of 1 to 10 μm at the input. The input and output signals are measured for 300s and used to construct the FRF according to Welch's method [27].

The moving mass has a fly height of 0.18 ± 0.05mm corresponding to a volume of 0.2 mm ferrofluid per bearing and a total weight of 0.185kg. It is supported by three square ferrofluid bearings using the magnet Q-20-20-05-N from Supermagnete.

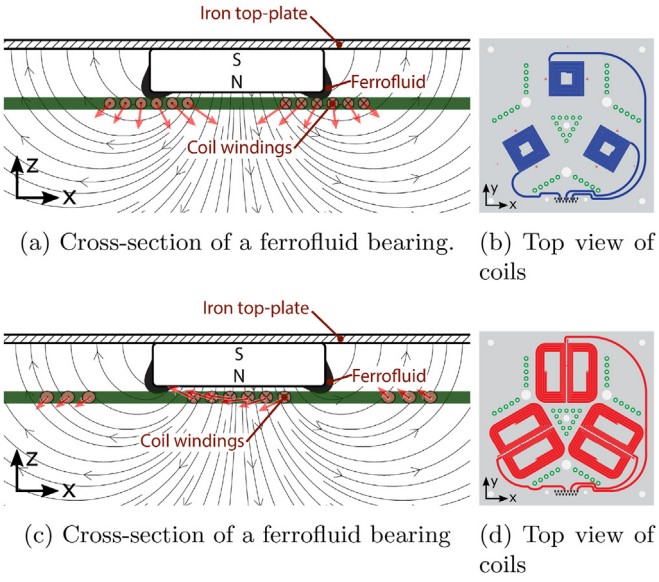


(a) Cross-section of a ferrofluid bearing. (b) Top view of coils

(c) Cross-section of a ferrofluid bearing (d) Top view of coils

**Fig. 6.** The coils create a resultant out-of-plane(6a) and in-plane(6c) force as a result of the Lorentz forces and designed coil configuration. Fig. 6d and b shows the coil configuration from a top-view, with the three coil-sets corresponding to three ferrofluid bearings.

### 3.3. Damping coefficient by dynamic response

The system can be described as a mass-spring-damper system with transfer function (27), using the results from section 2.3 that a ferrofluid bearing behaves like a linear viscous damper. Where the mass is denoted as $m$, the damping coefficient as $c$ and the stiffness value as $k$.

$$\frac{X_o(s)}{F(s)} = \frac{1}{ms^2 + cs + k} \tag{27}$$

Fig. 7 shows the response of the system discribed by equation (27) in the case of an over- and underdamped mass-damper-spring system. At low frequencies the stiffness of the system will determine the dynamic behaviour, while at high frequencies the inertia of the moving mass will dominate. The damper-line limits the resonance peak height, by dissipating energy as a result of the damping forces.

The value of system parameters can be determined by finding the pole locations in the frequency response function(FRF). According to equation (27), the pole location of the damping is described by equation (28).

$$\omega_{cm} = \frac{c}{m} \tag{28}$$

However, the ferrofluid bearing system is underdamped, with a pole expected at approximately 0.5Hz. The identification through a FRF suffers from limits in exposure time and assumptions made in the signal processing, leading to inaccurate measurements at low frequencies. Therefore a control stiffness $k$ is added to the system expanding it to a mass-spring-damper system as presented in Fig. 7.

The damping coefficient can be expressed in system parameters according to (29). It is now expressed in one known parameter, mass; one chosen parameter, stiffness; and one unknown parameter, damping ratio.

$$c = 2\zeta\sqrt{km} \tag{29}$$

The damping ratio can be related to the Q-factor, which can be defined as the ratio of stored energy to dissipated energy.

$$\zeta = \frac{1}{2Q} \tag{30}$$

Combining (29) and (30) gives:

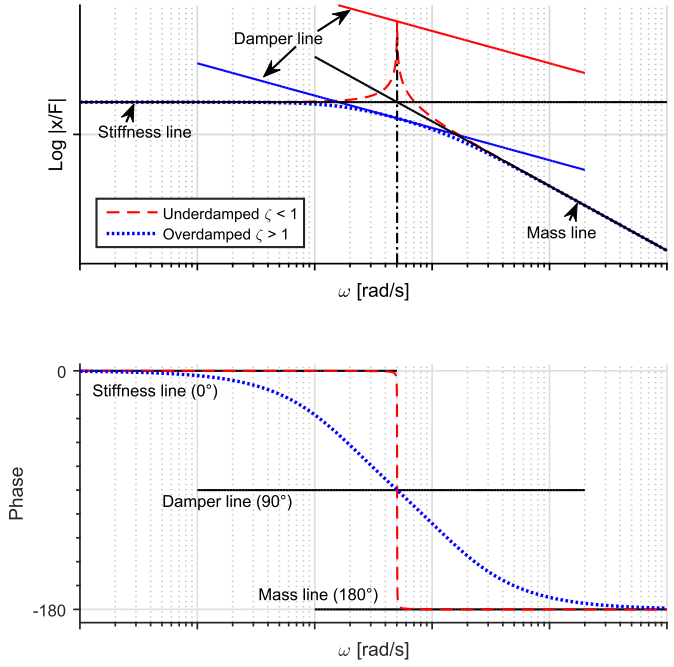


**Fig. 7.** This figure shows a typical response for an underdamped ($\zeta < 1$) and an overdamped ($\zeta > 1$) mass-spring-damper system. At low frequencies the stiffness of the system dominates, while at high frequencies the inertia dominates. The amplitude of the resonance is related to the dissipated energy of the system, a result of the damping forces.

$$c = \frac{\sqrt{km}}{Q} \tag{31}$$

For measurement purposes the Q-factor can be defined as the frequency-to-bandwidth ratio of the resonator, where $f_r$ is the resonant frequency and $\triangle f$ is the full width at half maximum(FWHM) bandwidth.

$$Q = \frac{f_r}{\triangle f} \tag{32}$$

In the system used for this research, stiffness is created by adding a control gain($K_p$) in the closed-loop control scheme. Fig. 8 shows the block diagram of a typical closed-loop feedback controller, where $G(s)$ is the plant model and $K_p$ the control stiffness. The transfer function describing the response of this system is shown in (33).

$$\frac{X_o(s)}{X_i(s)} = \frac{G(s)C(s)}{1 + G(s)C(s)} \tag{33}$$

The plant of a ferrofluid bearing can be modelled as a mass-damper system and the closed-loop transfer function becomes (34).

$$\frac{X_o(s)}{X_i(s)} = \frac{K_p}{ms^2 + cs + K_p} \tag{34}$$

Which can be rewritten in the form of (27), by noting that $F(s) = K_p X_i(s)$.

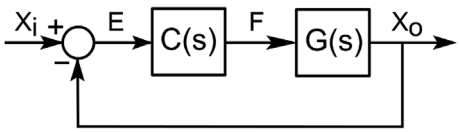


**Fig. 8.** The block diagram of closed-loop feedback control, with plant model $G(s)$ and controller gain $K_p$. $X_i(s)$ is the reference signal, $E(s)$ is the error signal, $F(s)$ is the plant input signal and $X_o(s)$ is the output signal.

**Table 1**
This table shows the measured parameters and modelled in-plane damping coefficient of a ferrofluid bearing. The damping coefficient is calculated according to (22).

| | Quantity | Value |
|---|---|---|
| System: | $\eta$ [kgm$^{-1}$s] | 150 ± 15× $10^{-3}$ |
| | $A$ [m$^2$] | 220 ± 10× $10^{-6}$ |
| | $h$ [m] | 0.18 ± 0.05× $10^{-3}$ |
| | $c$ [Nsm$^{-1}$] | 2.2 ± 0.8 |

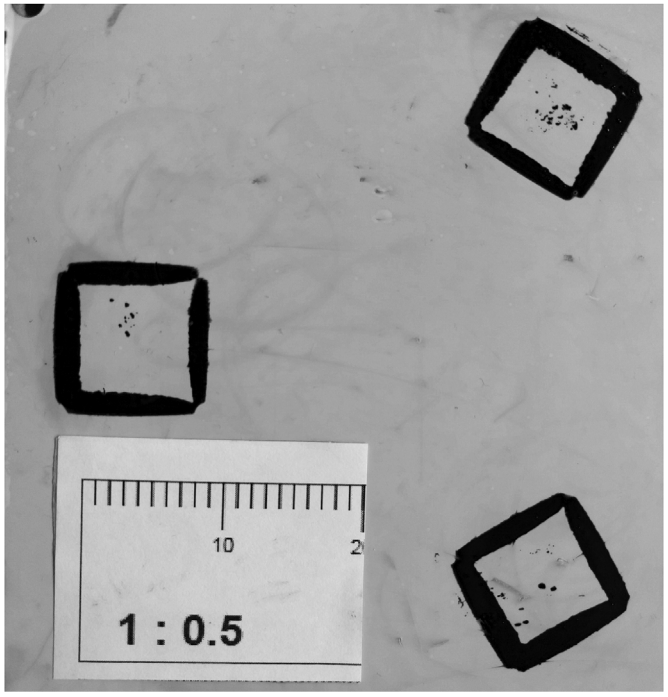


**Fig. 9.** The imprint left by the ferrofluid bearings on a smooth surface compared to a 1:0.5 mm scale. In this image the red and green has been filtered out to increase contrast between the ferrofluid and background.

$$\frac{X_o(s)}{F(s)} = \frac{X_o(s)}{K_p X_i(s)} = \frac{1}{ms^2 + cs + K_p} \tag{35}$$

The Q-factor can now be measured according to (32).

## 4. Results

The damping coefficient that is calculated using equation (22), is presented in Table 1 together with the different values that are used to calculate the coefficient (see Fig. 9 for surface area). The predicted damping coefficient for the three bearings in the system is 2.2 ± 0.8Nsm$^{-1}$.

Fig. 10 shows the frequency response for closed-loop control stiffness values, ranging from 5 × $10^3$ up to 30 × $10^3$Nm$^{-1}$. Fig. 11 shows the different damping coefficients corresponding to the different control stiffnesses shown in of Fig. 10. Fig. 12 shows the effect of different input amplitudes on the damping coefficient for a constant stiffness. The measured damping coefficient of the complete system based on the dynamic response is found to be 2.97 ± 0.45Nsm$^{-1}$.

## 5. Discussion

From the measured dynamic behaviour of the system presented in Fig. 10, it has been shown that the system can be considered to be a perfect mass-spring-damper system. At low frequencies the response converges to the applied control stiffness, while at high frequencies the responses converge to the inertia of the mass. In-between, a resonance peak is present of which the peak height decays as would be expected from a viscous damper model.

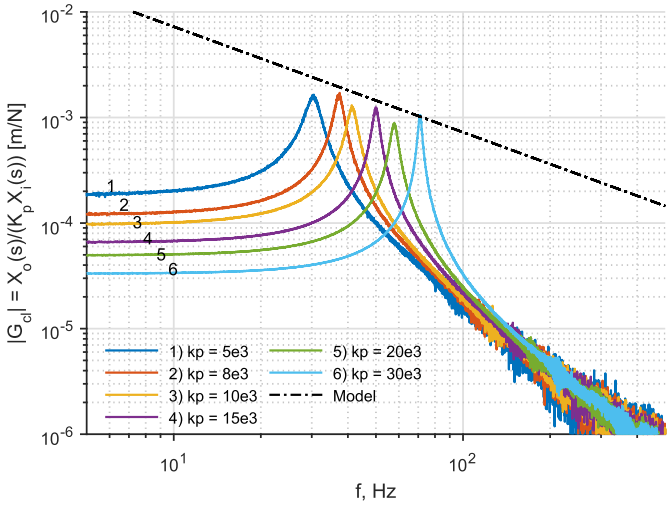


**Fig. 10.** The frequency response of the closed-loop system with added control stiffness $K_p$. The black dotted line resembles the modelled damping coefficient. The peaks being close to the black dotted lines demonstrates that the model is in line with the measurements.

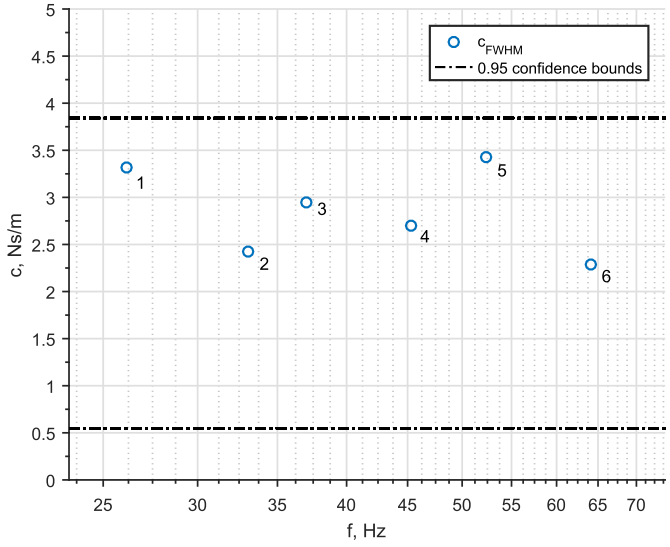


**Fig. 11.** The damping coefficient determined via FWHM are displayed as a function of the resonance bandwidth. The dotted line represent the 0.95 confidence bound of the model. The numbers correspond with the measurement labels of Fig. 10.

The uncertainty of the modelled damping coefficient presented in Fig. 11 is the result of multiple measurement uncertainties. The figure furthermore shows no non-linearities in the trend or magnitude of the damping coefficients. Some differences can be explained by the assumed constant viscosity, which is not necessarily the case for a ferrofluid [20]. Fig. 12 shows that the damping coefficient stays constant for constant stiffness and varying input amplitude and therefore varying input sliding velocity. This altogether demonstrates that the assumption of a constant viscosity for a ferrofluid bearing is fair under these conditions.

The peak heights in Fig. 10 scales with the stiffness as expected over the measured region. This implies that the damping coefficient stays constant for the used input amplitudes and stiffness. However, the

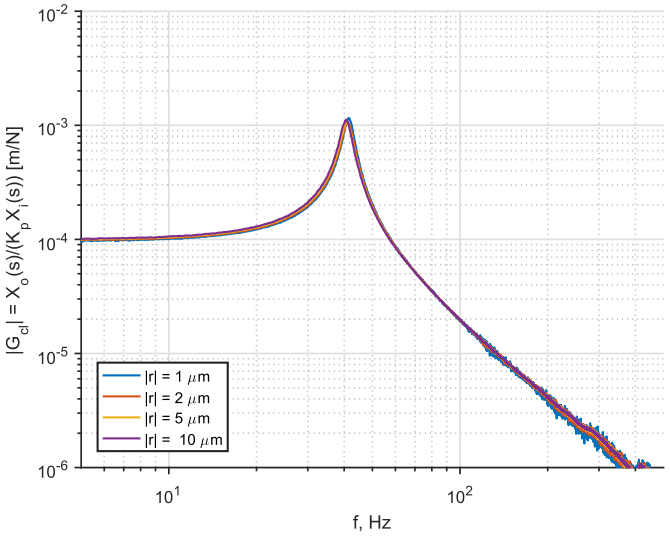


**Fig. 12.** The effect of a variation in the input signal amplitude on the frequency response with a constant stiffness of $K_p = 10 \times 10^3$. The amplitude varies from 1 up to 10 μm. This proves the linearity for 1–10 μm.

measured damping constant is systematically higher than the modelled coefficient. This implies that a systematic error or another undescribed effect occurs in the method of determining the modelling parameters. A likely candidate for a systematic error is the fluid film thickness, due to the small distance and lack of stiff connection.

The results are measured for stroke lengths up to ~ 1 m, as a result the maximal input amplitude of 10 μm with a maximal Q-factor of ~ 100. So for large stroke($\ell \gg 1mm$) additional experiments need to be performed.

The theoretical bearing model presented in this paper requires that the magnetic body force is strong enough to keep the ferrofluid in place. For large speeds, it might be possible that the body force is not large enough to pull back the fluid. In the case of a ferrofluid pocket bearing, this results in leakage of air through the seal, resulting in a permanent change in fly height.

## 6. Conclusion

A ferrofluid bearing is a low-cost, relatively simple, concept that has been proven to have no discernible stick-slip effects and is therefore well suited for precision positioning systems.

The model as presented in Ref. [17] is expanded to include the magnetic body force, ensuring a Pouiseuille flow counteracting the Couette flow resulting in no significant fluid-loss during motion. The resulting flow field is used to derive the in-plane damping coefficient of a ferrofluid bearing. A ferrofluid bearing has no in-plane stiffness, by adding a control stiffness it's dynamic behaviour can be modelled as a mass-damper-spring system.

The ferrofluid bearings in the identified system behave like a linear viscous damper for the utilized input amplitudes. Although the viscosity is non-linear as a function of the speed, the expanded model proves a valid approach at quantifying the damping coefficient of a ferrofluid bearing.

The validity of the friction model demonstrates that the load capacity is affected by the translational motion of the bearing. The magnetic body force used for creating load capacity is then additionally used for keeping the fluid in place. This results in a lower net load capacity during translation. It is important to take this effect into account during the design of the bearing.

The presented model allows for better design of precision positioning systems using FF bearings.

## Acknowledgements

This research has been supported by the Dutch TKI maritime funding program.

## Appendix A. Supplementary data

Supplementary data related to this article can be found at https://doi.org/10.1016/j.precisioneng.2018.05.013.

## References

[1] Garagić Denis, Srinivasan Krishnaswamy. Adaptive friction compensation for precision machine tool drive. Contr Eng Pract 2004;12(11):1451–64. https://doi.org/10.1016/j.conengprac.2003.10.006. ISSN 09670661.
[2] Rosensweig Ronald E. Bearing arrangement with magnetic fluid defining bearing pads. 1971.
[3] Ridler Keith Douglas, Gosling Alexander Bennet, Edge Gordon Malcom. Linear bearing for parallel tracking arm. 1977.
[4] Sudo Seiichi, Takaki Yuji, Hashiguchi Yasunari, Nishiyama Hideya. Magnetic fluid devices for driving micro machines. JSME International Journal Series B 2005;48(3):464–70. https://doi.org/10.1299/jsmeb.48.464. ISSN 1340-8054.
[5] Uhlmann E, Bayat N. High precision positioning with ferrofluids as an active medium. CIRP Ann - Manuf Technol 2006;55(1):415–8. https://doi.org/10.1016/S0007-8506(07)60448-X. ISSN 00078506.
[6] Simon van Veen. Planar ferrofluid bearings for precision stages. PhD thesis, MSc thesis, Delft University of Technology; 2013.
[7] Assadsangabi B, Tee MH, Takahata K. Ferrofluid-assisted levitation mechanism for micromotor applications. Transducers & eurosensors XXVII: the 17th international conference on solid-state sensors. Actuators and Microsystems; 2013. p. 2720–3.
[8] Assadsangabi Babak, Tee Min Hian, Takahata Kenichi. Electromagnetic microactuator realized by ferrofluid-assisted levitation mechanism. Journal of Microelectromechanical Systems 2014;23(5):1112–20. https://doi.org/10.1109/JMEMS.2014.2305112.
[9] Café Max. Nanometer precision six degrees of freedom planar motion stage with ferrofluid bearings Master thesis Delft University of Technology; 2014
[10] Georges Stefan, Lampaert Emile, Café Max, Ostayen Ron A J van, Spronck Jo W. (2+4) DOF precision motion stage with ferrofluid bearings 2016 Spring Meeting: Precision Mechatronic System Design and Control 2016. p. 7–10.
[11] Habib Haris. Design of a three Degrees of Freedom planar precision stage using a single Position Sensitive Detector Master thesis Delft University of Technology; 2015
[12] Georges Stefan, Lampaert Emile, Habib Haris, Spronck Jo W, Ostayen Ron A J van. XY360 planar positioning stage with ferrofluid bearings. DSPE-Conference 2016. 2016. p. 57–61.
[13] Mok Gihin. The design of a planar precision stage using cost effective optical mouse sensors. Msc thesis, Delft University of Technology; 2015.
[14] Alvarez-Aguirre Alejandro, Mok Gihin, Hassan HosseinNia S, Spronck Jo. Performance improvement of optical mouse sensors: application in a precision planar stage. 2016 international conference on manipulation, automation and robotics at small scales, MARSS 2016 2016. https://doi.org/10.1109/MARSS.2016.7561698.
[15] van Moorsel Len. A planar precision stage using a single image sensor. Msc thesis, Delft University of Technology; 2017.
[16] Huang Wei, Shen Cong, Wang Xiaolei. Study on static supporting capacity and tribological performance of ferrofluids. Tribol Trans 2009;52(5):717–23. https://doi.org/10.1080/10402000902913337. ISSN 1040-2004 http://www.tandfonline.com/doi/abs/10.1080/10402000902913337.
[17] Georges Stefan, Lampaert Emile. Planar ferrofluid bearings modelling and design Principles Msc thesis, MSc thesis Delft University of Technology; 2015
[18] Georges Stefan, Lampaert Emile, Spronck Jo W, Ostayen Ron A J van. Load and stiffness of a ferrofluid pocket bearing. The 17th nordic symposium on tribology. 2016. p. 11.
[19] Lampaert SGE, Spronck JW, van Ostayen RAJ. Load and stiffness of a planar ferrofluid pocket bearing. Proc IME J J Eng Tribol 2018;232(1):14–25. https://doi.org/10.1177/1350650117739200. ISSN 1350-6501 http://journals.sagepub.com/doi/10.1177/1350650117739200.
[20] Odenbach Stefan. Magnetoviscous and viscoelastic effects in ferrofluids. Int J Mod Phys B 2000;14(16):1615–31. https://doi.org/10.1142/S0217979200001692. ISSN 0217-9792.
[21] Shliomis MI. Effective viscosity of magnetic fluids. Sov Phys - JETP 1972;24(6):1291–4. ISSN 00319015.
[22] Albert Einstein. On the motion of small particles suspended in a stationary liquid, as required by the molecular kinetic theory of heat. Ann Phys 1905;322(8):549–60. https://doi.org/10.1002/andp.19053220806. ISSN 1521-3889.
[23] Odenbach Stefan, Thurm Steffen. Magnetoviscous effects in ferrofluids. In: Odenbach Stefan, editor. *Ferrofluids SE - 10*, volume 594 of *lecture Notes in physics*. Springer Berlin Heidelberg; 2002. p. 185–201. ISBN 978-3-540-43978-3 https://doi.org/10.1007/3-540-45646-5_10.
[24] Odenbach Stefan, Störk H. Shear dependence of field-induced contributions to the viscosity of magnetic fluids at low shear rates. J Magn Magn Mater 1998;183(12):188–94. https://doi.org/10.1016/S0304-8853(97)01051-2. ISSN

0304-8853 http://www.sciencedirect.com/science/article/pii/S0304885397010512.
[25] Jordan Peter C. Association phenomena in a ferromagnetic colloid. Mol Phys January 2015;25:961–73. https://doi.org/10.1080/00268977300100821. 1973. ISSN 0026-8976.
[26] Yu Zubarev Andrey, Odenbach Stefan, Fleischer J. Rheological properties of dense ferrofluids. Effect of chain-like aggregates. J Magn Magn Mater 2002;252(0):241–3. ISSN 0304-8853 https://doi.org/10.1016/S0304-8853(02)00674-1http://www.sciencedirect.com/science/article/pii/S0304885302006741.
[27] Welch Peter D. The use of fast fourier transform for the estimation of power spectra: a method based on time averaging over short, modified periodograms. IEEE Trans Audio Electroacoust 1967;AU-15(2):70–3.